

Radar shielding experiments by composite bilayer magnetic systems

Jaume Calvo-de la Rosa, Jesús López-Sánchez, Joan Manel Hernández, Pilar Marín, and Javier Tejada

Abstract—A strong increase of the reflection loss (from 25 up to 35 dBs) and an extension of the absorption bandwidth up to 20% under far-field real radar conditions are experimentally reported in this work by creating a functional bilayer system. Each layer consists of a composite material, typically a dielectric matrix filled with magnetic entities (powder or wires). Combining the two types of materials into a bilayer structure has shown unprecedented improvements in microwave absorption capacities compared to the former absorption of each layer. The potential of random magnets to create thin broadband absorbers is also demonstrated. The capacity to improve the shielding behavior is strongly related to each layer's permittivity, permeability, and thickness. This provides strong control over the design of novel materials for stealth applications.

Index Terms—bilayers, functional composites, magnetic materials, radar

I. INTRODUCTION

RADIO detection and ranging (radar) technology has been extensively used during the last century. Nonetheless, this technology has notably evolved, and it is still attracting much attention in fields like aviation [1,2], marine navigation [3,4] or space exploration [5], for instance. Many scientific and engineering efforts are paid to the generation, control, and detection of microwaves to improve the capacities of this technology. However, on the other side, stealth technology fights for the opposite goal: making objects

Jaume Calvo-de la Rosa, Joan Manel Hernández, and Javier Tejada thank the U.S. Air Force Office of Scientific Research (AFOSR) [grant number FA8655-22-1-7049] for their financial support. Joan Manel Hernández thanks the Departament de Recerca i Universitats de la Generalitat de Catalunya [grant number 2021SGR00328]. Jesús López-Sánchez acknowledges the financial support from grant RYC2022-035912-I funded by MCIU/AEI/10.13039/501100011033 and by the European Social Fund Plus (ESF+). Pilar Marín acknowledges the financial support from the Spanish Ministry of Economic Affairs and Digital Transformation through the project PID2021-123112OB-C21-MICINN, to the Community of Madrid NanomagCOST project (S2018/NMT-4321). Finally, all the authors would also like to thank the enterprise AMES S.L. for providing the necessary materials.

(Corresponding author: Jaume Calvo-de la Rosa).

Jaume Calvo-de la Rosa, Joan Manel Hernández and Javier Tejada are with Departament de Física de la Matèria Condensada at Universitat de Barcelona, c/Martí i Franquès 1, 08028 Barcelona (Spain). Jaume Calvo-de la Rosa and Joan Manel Hernández are member of the Institut of Nanociència i Nanotecnologia (IN2UB) at the Universitat de Barcelona as well. (e-mail: jaumecalvo@ub.edu).

Jesús López-Sánchez and Pilar Marín are with the Instituto de Magnetismo Aplicado (IMA-UCM-ADIF), 28230 Madrid (Spain), and Departamento de Física de Materiales, Facultad de Físicas, Universidad Complutense de Madrid (UCM), 28040 Madrid (Spain).

invisible to radar detection [6]. Metamaterials or radar-absorbing materials (RAMs) are two different approaches to designing materials that prevent the incident waves from being reflected from the object. RAMs may also be used for other purposes, like protecting critical systems from foreign electromagnetic (EM) radiation, such as strategic computing, control, or telecommunication structures. The appearance of electromagnetic pulse (EMP) weapons [7,8] makes EM protection a more sensitive issue day by day.

A large variety of materials have been studied as RAMs, ranging from ceramics, metals, or even polymers. In this scenario, carbon-based structures are a class of materials that are gaining momentum due to their low density, strong dielectric loss, and good mechanical properties [9,10]. Nonetheless, they are somehow limited by the complexity of their preparation and scalability. On another hand, ferrites have shown excellent shielding capacities while keeping a good balance between the above-mentioned properties. More particularly, hexaferrites (typically $\text{BaFe}_{12}\text{O}_{19}$ or $\text{SnFe}_{12}\text{O}_{19}$) have shown particularly good microwave attenuation capacities [11,12]. Finally, soft magnetic metals and alloys have also attracted attention due to their high saturation magnetization and magnetic susceptibility. Amorphous magnetic microwires have extensively been reported as excellent microwave absorbers, due to the strong attenuation they show and their capacity to be modified for different requirements [13–15]. Their absorption frequency has been controlled through the wire length [13]. These materials were patented [16] and industrially exploited for electromagnetic shielding applications for years.

Recent theoretical studies [17–19] postulate random magnetic materials as excellent candidates for microwave absorption. In the same direction, recent experiments have verified that barium hexaferrite-based nanocomposites behave as random-anisotropy magnets [20], converting them into excellent candidates as broadband microwave absorbers. These nanocomposites are understood as a collection of nanocrystallites, of similar size to the domain wall width, each of them with a randomly oriented anisotropy axis. Both anisotropy and exchange interactions govern the magnetization dynamics; however, under these conditions, anisotropy becomes dominant over exchange interaction. The conclusions reported in [20] state that these ceramic random-anisotropy magnets show improved broadband absorption capacities in thin (sub-millimetric) layer systems.

The present work provides experimental evidence of a significant increase in the radar absorption capabilities of a well-known type of magnetic microwire sheets by combining

> REPLACE THIS LINE WITH YOUR MANUSCRIPT ID NUMBER (DOUBLE-CLICK HERE TO EDIT) <

them with an additional composite layer. This secondary layer is made of a dielectric matrix and a magnetic powder filler, either metallic or hexaferrite-based nanocomposites. The data reported here also provides a deep analysis of the effect that the creation of the bilayer configuration has on the absorption bandwidth.

II. MATERIALS AND METHODS

A. Materials and synthesis

In this work, we make use of multiple magnetic materials, either powder or wire-like. On one hand, we used own-synthesized barium hexaferrite (BaHF) and hexaferrite-based nanocomposites, which have been proven to behave as random magnets [20]. These pure and composite hexaferrite compounds were synthesized through a conventional co-precipitation process [21]. Stoichiometric amounts of the necessary metal salt precursors [$\text{Ba}(\text{NO}_3)_2$, $\text{Fe}(\text{NO}_3)_3 \cdot 9\text{H}_2\text{O}$, $\text{Cu}(\text{NO}_3)_2 \cdot 3\text{H}_2\text{O}$ and $\text{Mn}(\text{NO}_3)_2 \cdot 4\text{H}_2\text{O}$, all from Sigma Aldrich as received] were dissolved in distilled water and stirred for two hours. Once the reactants were dissolved, a 2M NaOH (Sigma Aldrich, as received) solution was incorporated into the solution dropwise until a basic pH of ~ 10 was achieved. In these basic conditions, precipitation occurs. The solution was stirred while heated at 80°C for two additional hours to facilitate the completion of the reaction. The obtained suspension was subjected to 4 centrifugation cycles of 10 minutes at 3000 rpm. Between each cycle, the remaining solid product was washed with a mixture of water and ethanol at 50% in volume to remove the remaining undesired products from the previous steps. The obtained solid was then dried for 24 hours at 80°C and ground with a mortar before a final calcination process of 1 hour at 900°C , which activates the solid-state diffusion to form the desired ferrite. The ferrite is finely ground again to obtain a fine and homogenous powder.

On the other hand, metallic soft magnets are also considered in this study. Pure iron and a type of iron-based soft magnetic composite powder samples were provided by the enterprise AMES S.L. The first type of material (which we will refer to as soft magnetic material, SMM, according to literature) consists of pure iron particles with $100\ \mu\text{m}$ in diameter. This powdered material stands out for its high magnetic permeability. The other material (referred to as soft magnetic composite, SMC) consists of $200\ \mu\text{m}$ particles made of an iron core and an isolating phosphate-based isolating shell. This isolating shell prevents percolation between particles and the subsequent creation of eddy currents, which lead to power losses. This material can maintain a high permeability upon higher frequencies. The complete chemical, structural, and magnetic characteristics of these two materials may be found at [22].

The last class of materials used are magnetic microwires, which consist of an iron core wire surrounded by a glass coating. These microwires were prepared by the Taylor technique [23]. The inner core is made of $\text{Fe}_{89}\text{BSi}_3\text{Mn}_4$ and has a diameter of $12\ \mu\text{m}$. The total diameter is $20\ \mu\text{m}$, while the wires' length is 1 mm.

Table I below summarizes and identifies all these materials, which are used as fillers in our composites:

TABLE I
LIST AND ID OF THE DIFFERENT MATERIALS USED IN THIS WORK

ID	Material
MW	Amorphous magnetic microwires
HF	Own synthesized BaHF
HF-Cu	Own synthesized BaHF + Cu nanocomposite
HF-Mn	Own synthesized BaHF + Mn nanocomposite
SMM	Pure iron particles
SMC	Iron particles with a phosphate-isolating shell

In addition to the magnetic fillers, paint was also used as a dielectric isolating matrix for our samples, where fillers were dispersed. Titan's Unilak white water enamel was used to disperse the powder samples, while Hempel primer undercoat was used for the microwires.

B. Sheets preparation

The magnetic powders and wires were mixed with the corresponding amount of paint and deposited into $25\ \text{cm} \times 25\ \text{cm}$ polyester sheets to fabricate layer-type samples. In this work, we aim to analyze the effect that multiple design factors (such as the chemical nature of the filler) have on their radar absorption capacities. Table II lists the characteristics of the collection of sheets prepared for this work. In addition to the filler's chemical nature, we also inspect the effect of another crucial geometrical aspect: the layer's thickness. As it may be seen, for each type of filler we have prepared three sheets with different thicknesses, to which we refer as small (S), medium (M), and large (L). All 16 fabricated samples and their main characteristics are listed in Table II. Given that the weight filling factor (ff_w) is constant, the sample identifiers follow the next structure: filler_thickness, being the thickness represented by its class type (S, M, or L).

TABLE II
LIST AND ID OF THE DIFFERENT MATERIALS USED IN THIS WORK

#	ID	Matrix	Filler	ff_w (%)	Thickness (mm)
1	MW	Hempel primer undercoat	MW	1.2	0.280
2	HF_S	Titan's Unilak paint	HF	4.0	0.290
3	HF_M	Titan's Unilak paint	HF	4.0	0.580
4	HF_L	Titan's Unilak paint	HF	4.0	0.720
5	HF_Cu_S	Titan's Unilak paint	HF_Cu	4.0	0.340
6	HF_Cu_M	Titan's Unilak paint	HF_Cu	4.0	0.560
7	HF_Cu_L	Titan's Unilak paint	HF_Cu	4.0	0.820
8	HF_Mn_S	Titan's Unilak paint	HF_Mn	4.0	0.290
9	HF_Mn_M	Titan's Unilak paint	HF_Mn	4.0	0.540
10	HF_Mn_L	Titan's Unilak paint	HF_Mn	4.0	0.740
11	SMM_S	Titan's Unilak paint	SMM	4.0	0.320
12	SMM_M	Titan's Unilak paint	SMM	4.0	0.480
13	SMM_L	Titan's Unilak paint	SMM	4.0	0.770
14	SMC_S	Titan's Unilak paint	SMC	4.0	0.380
15	SMC_M	Titan's Unilak paint	SMC	4.0	0.500
16	SMC_L	Titan's Unilak paint	SMC	4.0	0.560

C. Electromagnetic characterization

All the samples' reflection loss (R_L) was measured inside an anechoic chamber equipped with broadband electromagnetic radiation absorbers (EMC-24PCL, ETS-Lindgren) and plates to prevent edge effects. The absorbing medium consists of a pyramidal polyurethane foam, designed with a specific geometry to minimize losses and attenuation of the incident wave, as well as to reduce noise that could affect measurements. Samples were subjected to a metallic plate to ensure total reflection. The signal was emitted by one antenna, reflected by the metallic plate behind the sample, and detected back by the other antenna (S_{21} measurement). The EMCO 3160-07 horn antennas, positioned under far-field conditions relative to the optimized absorbing paint, were connected to an Agilent E8362B PNA Series Network Analyzer outside the anechoic chamber to generate and detect the reflected signals. Under these conditions, the transmission of electromagnetic waves can be considered as plane waves. 1601 points were measured between 0.5 and 18 GHz. This measurement system is schematized in Fig. 1.

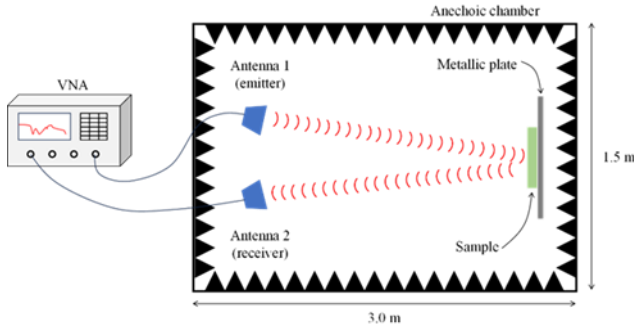


Fig. 1. Schematic representation of the far field radar measurements done inside the anechoic chamber.

III. RESULTS AND DISCUSSION

We start by measuring, individually, the sheets listed in Table II. In Fig. 2 we show, as an example case, the data corresponding to the MW sample together with the thinnest sheet of each composition. MW absorbs 25 dB at ~ 9.5 GHz, in good agreement with previous reports of the same material [24]. On the other hand, none of the sheets containing hexaferrite or metallic powder show significant absorption in this frequency range. The same full reflection behavior was also observed for the M and L sheets. With these results, we conclude, without doubt, that the sheets containing hexaferrite or metallic powder are non-absorbent in this frequency range. This does not mean that these materials cannot be radar absorbers, but that they do not absorb in this frequency range for these specific characteristics (i.e., composite layers with $ff_w = 4\%$ and thicknesses between ~ 0.25 and 0.75 mm). Indeed, pure hexaferrite-based samples have been recently proven to absorb in this frequency range [20].

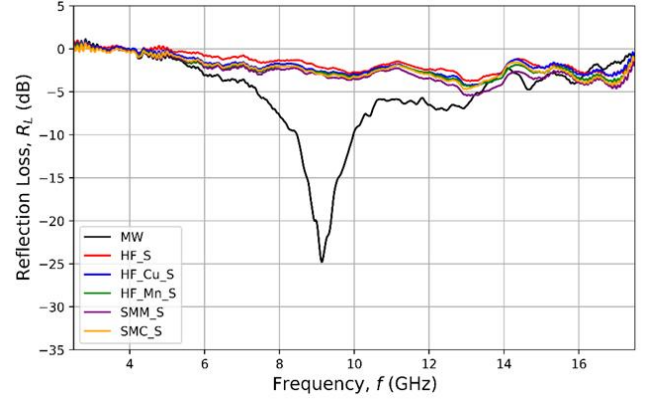


Fig. 2. Experimental R_L spectra, measured inside an anechoic chamber, for sample MW (black), HF_S (red), HF_Cu_S (blue), HF_Mn_S (green), SMM_S (purple), and SMC_S (orange).

Once the response for each sheet is clear, we start combining our reference MW sample with an additional ceramic or metal-based sheet. To begin, Fig. 3 shows the obtained results when the MW reference sample is combined with an additional layer filled with HF, either pure or modified. The full spectrum is represented in the main left column, while a closer view of the peaks is provided in the supporting right-side column.

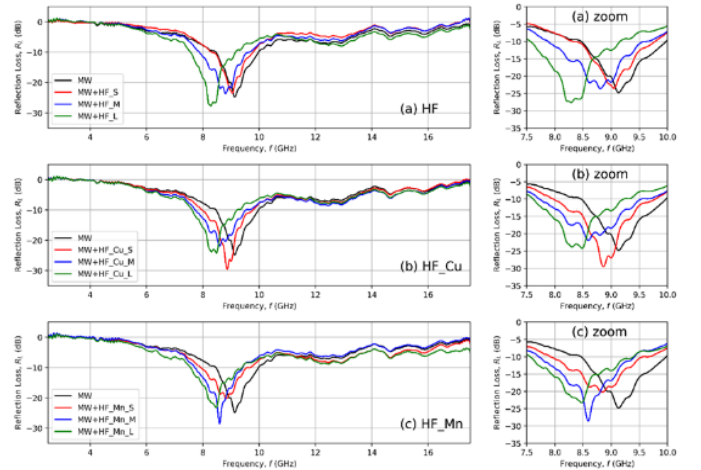


Fig. 3. Experimental R_L spectra, measured inside an anechoic chamber, for the addition of S (red), M (blue), and L (green) size distribution of (a) pure HF, (b) HF_Cu, and (c) HF_Mn powder. Left-side columns show the full spectrum between 2.5 and 17.5 GHz, while the right-side column provides an amplification close to the peaks.

In Fig. 3(a) we see how an additional HF-based layer behaves. It is observed that thin (S) layers do not produce an evident change in the absorption, but thicker sheets are capable of changing the response. Only for HF_L, we detect an improvement of the former MW absorption, moving R_L from -25 dB to -27 dB. In addition, it is observed a constant shift in the absorption frequency (i.e., the frequency position

> REPLACE THIS LINE WITH YOUR MANUSCRIPT ID NUMBER (DOUBLE-CLICK HERE TO EDIT) <

of the absorption peak) as a function of the second layer thickness. As may be expected, the larger the sheet thickness, the lower the absorption frequency is. The combination of MW+HF_L also seems to lead to a wider absorption compared to the former MW.

When HF_Cu is used instead of HF the effect is much more relevant, as Fig. 3(b) demonstrates. Even with the addition of HF_Cu_S, the R_L increases up to -30 dB. Contrary to the previous case, thicker layers do not improve the results. This is because of the different electromagnetic properties (dielectric permittivity and magnetic permeability) of the HF_Cu compared to HF, which requires a different optimum thickness to maximize absorption. On the other hand, the frequency shift as a function of thickness is consistent with the previous results.

Finally, moving to Fig. 3(c), we see that HF_Mn has an intermediate effect. In this case, the addition of a thin HF-Mn layer (S) reduces the original absorption, but it quickly increases when the intermediate sheet (M) is used. Then, it goes down again when the thickest (L) sheet is employed. A much clearer analysis of these behaviors is provided in Fig. 4, where three different absorption characteristics are systematically compared as a function of the second layer thickness.

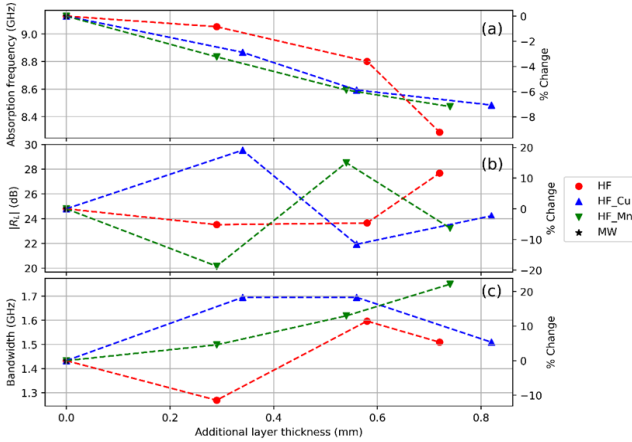


Fig. 4. Dependence of the (a) absorption frequency, (b) maximum absolute absorption, and (c) absorption bandwidth at -10 dB as a function of the thickness of the additional layer placed on top of the MW one (black star, at the origin) and its chemical composition, being HF (red circles), HF_Cu (blue up triangles) or HF_Mn (down triangles).

In Fig. 4(a), one may observe that the addition of the second layer displaces the absorption frequency to the lower region of the frequency domain. This is coherent given that the total thickness of the system is increased. Overall, with thin samples (< 1 mm) we can change the absorption frequency by 1 GHz in a continuous and controlled manner.

Fig. 4(b) shows the change in the absolute powder absorption. At first look, one might think there is no solid dependence on the second layer thickness. However, there are important points that must be mentioned. First, we can see that the maximum absorption happens only at a specific thickness. If the thickness is increased or reduced, the absorption falls.

Improvements of almost 30% (in dB scale) compared to the former MW absorption are achieved at specific conditions. This is in excellent agreement with the bilayer theory [25] which states that there is not a linear dependence between the absorption and the layers' thickness. This model, mathematically described by (1) and (2), defines the dependence of the R_L on each layer's permittivity, permeability, and thickness. The thickness must be optimized, according to the medium's electromagnetic properties, to achieve maximum absorption. Therefore, these results could even be improved with a proper design of the first layer's thickness.

$$Z = Z_0 \frac{\sqrt{\frac{\mu_1}{\epsilon_1}} \tanh\left[\left(\frac{j2\pi f d_1}{c}\right) \sqrt{\mu_1 \epsilon_1}\right] + \sqrt{\frac{\mu_2}{\epsilon_2}} \tanh\left[\left(\frac{j2\pi f d_2}{c}\right) \sqrt{\mu_2 \epsilon_2}\right]}{1 + \sqrt{\frac{\mu_1 \epsilon_2}{\mu_2 \epsilon_1}} \tanh\left[\left(\frac{j2\pi f d_1}{c}\right) \sqrt{\mu_1 \epsilon_1}\right] \tanh\left[\left(\frac{j2\pi f d_2}{c}\right) \sqrt{\mu_2 \epsilon_2}\right]} \quad (1)$$

$$R_L (\text{dB}) = -20 \log \left| \frac{Z/Z_0 - 1}{Z/Z_0 + 1} \right| \quad (2)$$

In good agreement with the observations made for Fig. 3, HF_Cu is the filler that increases the absorption earlier, with thinner added layers. Then, HF_Mn maximizes absorption for the intermediate (M) thickness layer, while HF is the one that requires thicker configurations to enhance the former absorption. These geometrical dependencies are in excellent agreement with [20], where random-anisotropy magnets are proved to be ideal candidates as broadband absorbers as thin coatings. This is of great importance for lightweight radar absorption applications.

Finally, Fig. 4(c) probably provides two of the most significant observations: (i) the addition of the second layer always expands the absorption bandwidth, and (ii) the random-anisotropy magnetic nanocomposites (HF_Cu and HF_Mn) have a better performance compared to the pure HF. These peak-broadening results also support the argument that identifies random-anisotropy magnets as ideal broadband microwave absorbers. Our experimental results prove an increase in the absorption bandwidth by up to 20% compared to the single MW layer. Again, we can see that there is an optimum thickness that maximizes the response, which depends on the specific electromagnetic properties of each sheet.

Now, we move to study the effect of the addition of a metal-based secondary layer instead of a ceramic-based one. In this case, we keep the MW sheet as the primary reference layer and we incorporate a secondary layer on top with a metallic soft magnet dispersed on it, either SMM or SMC. The results are depicted in Fig. 5.

> REPLACE THIS LINE WITH YOUR MANUSCRIPT ID NUMBER (DOUBLE-CLICK HERE TO EDIT) <

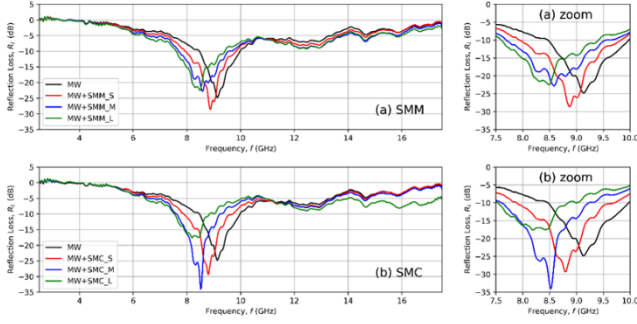


Fig. 5. Experimental R_L spectra, measured inside an anechoic chamber, for the addition of S (red), M (blue), and L (green) size distribution of (a) SMM and (b) SMC powder. Left-side columns show the full spectrum between 2.5 and 17.5 GHz, while the right-side column provides an amplification close to the peaks.

The addition of a metal-based layer has similar overall trends to those we have presented for the ceramic-based case. To start with the SMM filler, represented in Fig. 5(a), we can see that it may improve the former MW absorption with thin (S) added layers. Then, the absorption decreases. There is also a continuous displacement in frequency when the thickness is increased. On the other hand, the repercussion of adding an SMC is much stronger: the absorption can be enhanced up to -35 dB (which represents an enhancement of -10 dB) if the intermediate sheet (M) is used. Again, too large layers worsen the system performance. The frequency dependence of the peak position is again consistent with thickness. As we did with the ceramic-based cases, we provide a clearer analysis of the effect of the addition of the secondary layer in Fig. 6.

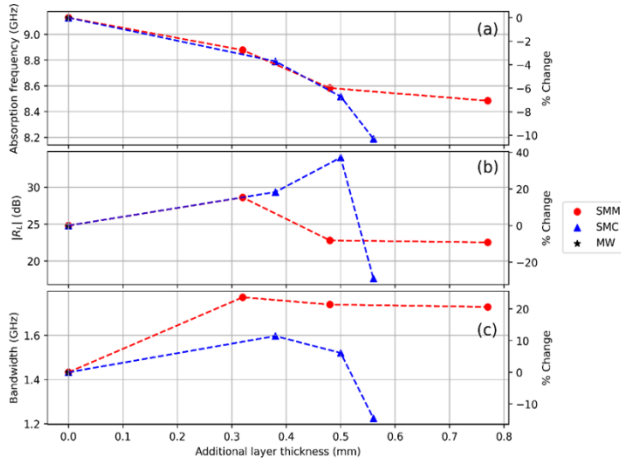


Fig. 6. Dependence of the (a) absorption frequency, (b) maximum absorption, and (c) absorption bandwidth at -10 dB as a function of the thickness of the additional layer placed on top of the MW one (black star, at the origin) and its chemical composition, being SMM (red circles) or SMC (blue up triangles).

Compared to the ceramic-based case, now we see that both materials absorb almost at the same frequency until the added layer exceeds 0.5 mm in thickness. Then, the effect of each material starts to be singular. Given that the SMC consists of a main Fe core surrounded by a phosphate-based isolating shell, the magnetic permeability is expected to be like the SMM one. This explains why the electromagnetic differences for thin layers are imperceptible. Fig. 6(a) shows how both types of layers shift the absorption peak identically with the S and M sheets; differences are not noticeable until L layers are used. The absorption frequency may be shifted up to 1 GHz with sub-millimetric secondary layers.

In terms of absolute absorption [Fig. 6(b)], SMC is a great candidate for improving the radar absorption of the system through the creation of a bilayer system. It may enhance the system's shielding capacities by 40% (in dB scale, from 25 to 35 dB) when a ~0.5 mm thick layer is incorporated. For layers thicker than 0.5 mm, the attenuation drops quickly. The pure SMM sample can increment the attenuation by almost 20%, reaching ~30 dB with 0.3 mm thick sheets.

SMC is clearly stated as the best option for increasing the power absorbed; however, looking at Fig. 6(c) it might be seen that SMM is the best option to enlarge the absorption bandwidth. The peak width at -10 dB is increased by 20% compared to the former MW absorption when a secondary SMM-based layer is incorporated. On the other hand, SMC (which had an exceptionally good response increasing the absorption intensity), is not capable of expanding the absorption bandwidth as much as SMM does. Thus, SMC is the best choice for situations when high R_L is required, but SMM is a better option when broadband absorption is required.

Overall, the absolute changes produced by the ceramic-based and the metallic-based additional layers are of the same order of magnitude. On the other hand, it must be said that, despite the metallic-based sheets reached the greatest increments in the powder absorbed (+40%, up to 35 dB), hexaferrite-based options offered a much more consistent performance. SMM and SMC produce strong improvements when for a narrow range of geometrical conditions, while hexaferrites perform well for a wider variety of thicknesses. On top of that, the addition of the secondary layer and the subsequent creation of bilayer systems has improved, simultaneously, the absolute powder absorbed, and the absorption bandwidth.

V. CONCLUSIONS

The results reported in this paper prove the high potential that bilayer systems have to improve the radar absorption capacities compared to traditional single-layer configurations. The experimental data reported here supports recent fundamental works that highlight their potential for stealth applications.

The use of hexaferrite-based layers emerges as an excellent and robust opportunity to improve, in a controlled manner, the total absorption of the systems. The immense potential that ceramic ferrites have to be chemically and structurally modified (which has a direct repercussion on their functional

behavior) is an excellent tool to adapt the electromagnetic response of the component. Random-anisotropy magnets, in the form of magnetic nanocomposites, have shown enhanced shielding capacities compared to pure barium hexaferrite. Both the reflection loss and the absorption bandwidth can be increased a 20% compared to the former single MW layer. Our experimental results support recent scientific findings that remark on the potential of random-anisotropy magnets as thin (<1 mm) broadband microwave absorbers. This converts these functional sheets made of random-anisotropy magnets into ideal candidates for lightweight electromagnetic shielding applications.

The use of soft metal-based functional layers has provided more significant improvements than the ceramic-based ones. However, their performance requires precise control of the layer thickness. SMC becomes an exceptional option to increase the powder absorbed, enhancing the R_L a 40%, from -25 to -35 dB. On the other hand, pure SMM is much better at widening the absorption peak, as it may lead to -10 dB absorption along 2 GHz.

Globally, the use of a secondary magnetic layer has improved the electromagnetic absorption capacities of a well-known single-layer absorbing material. Simultaneous improvements in the total powder absorbed and absorption bandwidth have been measured both for ceramic and metal-based composite layers. In addition, it must be highlighted that all the improvements have been achieved with sub-millimetric low-load ($ff_w = 4\%$) coatings, which might be of interest for lightweight applications. Finally, the strong potential to control these changes deserves to be mentioned as well. All the results obtained here have shown a strong dependence on the secondary layer thickness and the fillers' electromagnetic properties (which are the consequence of their chemical nature). A constant and robust modification of the absorption frequency has been measured, while the non-linear behavior between the R_L and the sample thickness and the electromagnetic response has been demonstrated.

REFERENCES

- [1] N. Al-Iqubaydhi et al., "Deep learning for unmanned aerial vehicles detection: A review," *Comput Sci Rev*, vol. 51, p. 100614, Feb. 2024, doi: 10.1016/J.COSREV.2023.100614.
- [2] M. Džunda, P. Džurovčin, P. Kaňavský, P. Korba, Z. Cséfalvay, and M. Hovanec, "The UWB Radar Application in the Aviation Security Systems," *Applied Sciences* 2021, Vol. 11, Page 4556, vol. 11, no. 10, p. 4556, May 2021, doi: 10.3390/AP11104556.
- [3] R. Morrow et al., "Ocean Circulation from Space," *Surveys in Geophysics* 2023 44:5, vol. 44, no. 5, pp. 1243–1286, Mar. 2023, doi: 10.1007/S10712-023-09778-9.
- [4] P. M. Atkinson, C. Zhang, and J. Lisowski, "Artificial Intelligence Methods in Safe Ship Control Based on Marine Environment Remote Sensing," *Remote Sensing* 2023, Vol. 15, Page 203, vol. 15, no. 1, p. 203, Dec. 2022, doi: 10.3390/RS15010203.
- [5] W. Guan, Y. Su, J. Li, S. Dai, C. Ding, and Y. Liu, "Applications of Ground-Penetrating Radar in Asteroid and Comet Exploration," *Remote Sensing* 2024, Vol. 16, Page 2188, vol. 16, no. 12, p. 2188, Jun. 2024, doi: 10.3390/RS16122188.
- [6] N. Shirke, V. Ghase, and V. Jamdar, "Recent advances in stealth coating," *Polymer Bulletin*, vol. 81, pp. 9389–9418, 2024, doi: 10.1007/s00289-024-05166-4.
- [7] Y. Xiong, X. Li, Z. Fan, B. Wang, Y. Zhang, and T. Wang, "Model-based Strong Electromagnetic Pulse Protection Optimization Design of Wheeled Armor," 2023 IEEE 6th International Conference on Electronic Information and Communication Technology, ICEICT 2023, pp. 135–138, 2023, doi: 10.1109/ICEICT57916.2023.10245896.
- [8] A. N. Skraparlis, K. S. Ntalianis, and N. Tsapatoulis, "A novel framework to intercept GPS-denied, bomb-carrying, non-military, kamikaze drones: Towards protecting critical infrastructures," *Defence Technology*, May 2024, doi: 10.1016/J.DT.2024.05.001.
- [9] F. Zhang et al., "Recent progress on carbon-based microwave absorption materials for multifunctional applications: A review," *Compos B Eng*, vol. 283, p. 111646, Aug. 2024, doi: 10.1016/J.COMPOSITESB.2024.111646.
- [10] J. López-Sánchez et al., "Generation of Defective Few-Layered Graphene Mesostructures by High-Energy Ball Milling and Their Combination with FeSiCuNbB Microwires for Reinforcing Microwave Absorbing Properties," *ACS Appl Mater Interfaces*, vol. 15, p. 3521, 2022, doi: 10.1021/ACSAMI.2C19886/ASSET/IMAGES/MEDIUM/AM2C19886_M007.GIF.
- [11] Y. He et al., "The combined sol-gel and ascorbic acid reduction strategy enabling Ba₂Co₂Fe₁₂O₂₂ hexaferrite/graphene composite with enhanced microwave absorption ability," *Mater Res Bull*, vol. 174, p. 112721, Jun. 2024, doi: 10.1016/J.MATERRESBULL.2024.112721.
- [12] W. Xu et al., "M-Type Ba-Hexaferrite Nanoplates with Exceptional Microwave Absorption Properties," *ACS Appl Electron Mater*, vol. 6, no. 4, pp. 2759–2766, Apr. 2024, doi: 10.1021/ACSAELM.4C00307/ASSET/IMAGES/LARGE/EL4C00307_0006.JPEG.
- [13] P. G. B. Gueye, J. López-Sánchez, E. Navarro, A. Serrano, and P. Marín, "Control of the Length of Fe₇₃.5Si₁₃.5Nb₃Cu₁B₉ Microwires to Be Used for Magnetic and Microwave Absorbing Purposes," *ACS Appl Mater Interfaces*, vol. 12, no. 13, pp. 15644–15656, 2020, doi: 10.1021/acsami.9b21865.
- [14] A. Moya, D. Archilla, E. Navarro, A. Hernando, and P. Marín, "Scattering of Microwaves by a Passive Array Antenna Based on Amorphous Ferromagnetic Microwires for Wireless Sensors with Biomedical Applications," *Sensors* 2019, Vol. 19, Page 3060, vol. 19, no. 14, p. 3060, Jul. 2019, doi: 10.3390/S19143060.
- [15] D. Archilla, J. López-Sánchez, A. Hernando, E. Navarro, and P. Marín, "Boosting the Tunable Microwave Scattering Signature of Sensing Array Platforms Consisting of Amorphous Ferromagnetic Fe_{2.25}Co_{72.75}Si₁₀B₁₅ Microwires and Its Amplification by Intercalating Cu Microwires," *Nanomaterials* 2021, Vol. 11, Page 920, vol. 11, no. 4, p. 920, Apr. 2021, doi: 10.3390/NANO11040920.
- [16] P. Marín Palacios, A. Hernando Grande, D. Cortina Blanco, J. J. Gomez Rebollo, and J. Calvo Robledo, "Electromagnetic radiation absorber based on magnetic microwires," *EP J* 675 217 A1, 2005
- [17] D. A. Garanin and E. M. Chudnovsky, "Random anisotropy magnet at finite temperature," *Journal of Physics Condensed Matter*, vol. 34, no. 28, p. 285801, Jul. 2022, doi: 10.1088/1361-648X/ac684a.
- [18] D. A. Garanin and E. M. Chudnovsky, "Absorption of microwaves by random-anisotropy magnets," *Phys Rev B*, vol. 103, no. 21, p. 214414, Jun. 2021, doi: 10.1103/PhysRevB.103.214414.
- [19] D. A. Garanin and E. M. Chudnovsky, "Nonlinear and Thermal Effects in the Absorption of Microwaves by Random Magnets," *Phys Rev B*, vol. 105, no. 6, p. 064402, 2021, doi: 10.1103/PhysRevB.105.064402.
- [20] J. Calvo-de la Rosa, J. M. Hernández, A. García-Santiago, J. M. Lopez-Villegas, and J. Tejada, "Barium Hexaferrite-based nanocomposites as random field magnets for microwave absorption," 2024. doi: 10.48550/arXiv.2402.14324.
- [21] J. Calvo-de la Rosa and M. Segarra, "Influence of the Synthesis Route in Obtaining the Cubic or Tetragonal Copper Ferrite Phases," *Inorg Chem*, vol. 59, no. 13, pp. 8775–8788, 2020, doi: 10.1021/acs.inorgchem.0c00416.
- [22] J. Calvo-de la Rosa, J. Tejada, and A. Lousa, "Structural and impedance spectroscopy characterization of Soft Magnetic Materials," *J Magn Magn Mater*, vol. 475, pp. 570–578, 2019, doi: 10.1016/j.jmmm.2018.11.085.

> REPLACE THIS LINE WITH YOUR MANUSCRIPT ID NUMBER (DOUBLE-CLICK HERE TO EDIT) <

- [23] A. Antonenko, S. Baranov, Larin VS, and A. Torkunov, "Natural ferromagnetic resonance in cast microwires covered by glass insulation," *Journal of Materials Science and Engineering*, vol. 247, p. 248, 1997.
- [24] P. Marín, D. Cortina, and A. Hernando, "Electromagnetic wave absorbing material based on magnetic microwires," *IEEE Trans Magn*, vol. 44, no. 11 PART 2, pp. 3934–3937, 2008, doi: 10.1109/TMAG.2008.2002472.
- [25] J. Calvo-de la Rosa et al., "New Approach to Designing Functional Materials for Stealth Technology: Radar Experiment with Bilayer Absorbers and Optimization of the Reflection Loss," *Adv Funct Mater*, vol. 34, no. 6, p. 2308819, Oct. 2023, doi: 10.1002/adfm.202308819.